DETECTION OF MAYA *SACBEOB* (SACBES) USING OPTICAL AND SAR IMAGERY IN NORTHERN PETÉN, MEXICO

A. LaRocque [1, *], B. Leblon [1], J. Ek [2], W.J. Folan [3]

[1] Faculty of Forestry and Environmental Management, University of New Brunswick, Fredericton (NB), E3B 5A3, CANADA - (larocque, bleblon)@unb.ca
[2] Department of Anthropology Western Washington University Bellingham (WA 98225), USA - ekg@wwu.edu
[3] Centro de Investigaciones Históricas y Sociales, Universidad Autónoma de Campeche, San Francisco de Campeche, Campeche, MEXICO - wijfolan@gmail.com

Commission III, WG III/7

KEY WORDS: Mayas, Archaeology, *Sacbe*s, Landsat, Alos-1 PalSAR, Sentinel-1.

ABSTRACT:
The pre-Contact Maya peoples build roads (*Sacbeob*) to facilitate movement between and within cities and surroundings. Given the dense forest cover in the Lowland Maya region now known as Yucatan, ground surveys of *sacbeob* are time-consuming and challenging to perform. Remote sensing can be a good alternative as it offers the advantages of extensive regional coverage, zero disturbances to cultural resources, and an opportunity to acquire data in less accessible areas on a cost-effective basis. LiDAR technology is highly valuable to detect man-made structures, but this technology is costly and is time-consuming to acquire data over a large area. Satellite imagery presents an alternative for mapping large areas. Previous studies documented linear features that could represent sections of *sacbeob* between Calakmul and El Mirador using Landsat-5 TM green, red, and near-infrared images (Folan et al. 1995). This study used Landsat-7 and Landsat-8 optical images having more bands and radar imagery (Sentinel-1 C-VH&VV, and Alos-1 PalSAR L-HH&HV) to connect *sacbeob* mapped by Folan et al. (1995) between three ancient Maya cities (Calakmul, El Mirador, and Uxul). Our results suggest that radar images with the capacity to penetrate dense forest cover can contribute to the identification and documentation of ancient road systems. Such a study provides an ideal starting point for targeted ground verification.

1. INTRODUCTION

Sacbeob (*Sacbe*s) or "white roads" (Shaw 2001, 2008) are raised roads that facilitate the movement of people and goods between pre-Hispanic Maya population centres (Bolles and Folan 2001, Shaw 2001) (Figure 1). Most of them are former causeways built or paved with white limestone, ranging from pebbles to powder. Given that delineating of *sacbeob* is essential to demonstrate the relationship between major cities and their distant subordinate centres, several *sacbeob* were already mapped, radiating out from major cities, like Calakmul (Folan et al. 1995) and El Mirador (Graham 1967). However, segments joining major Maya cities are rarely delineated, mainly because of the high density of the tropical canopy (Folan et al. 1995).

Given the dense forest cover in the interior Maya Lowlands, ground surveys of *sacbeob* are time-consuming and challenging to perform, especially over a long distance to cross, inside an inhospitable environment. Recently, airborne Light Detection and Ranging (LiDAR) scanning technology has been implemented to detect hidden Maya structures in Belize (Chase et al. 2010, 2011, 2013, Prufer et al. 2015, Thompson 2020), northern Yucatan (Magnoni et al. 2016), and Guatemala (Inomata et al. 2017, Canuto et al. 2018). Despite the details in detecting these structures, LiDAR technology is costly and covers relatively small areas. The same limitations can be applied to UAV imagery in remote regions such as Yucatan.

Satellite remote sensing could be a good alternative as it offers the advantages of extensive regional coverage, no disturbance of the area being mapped, and an opportunity for acquiring data in less accessible areas on a regular and cost-effective basis. As reviewed in Wiseman and El-Baz (2007) and Comer and Harrower (2013), both optical and radar images have been used for detecting and mapping several archaeological features across the world. With respect to ancient Maya features, Landsat-5 TM green, red and near-infrared images were used to map *sacbeob* segments and other archaeological features in some Maya sites in the Yucatan peninsula (Folan et al. 1995, Dominguez and Folan 1996, Sever 1998, Hixson 2013). More recent studies have implemented higher resolution optical imagery (such as Ikonos) to identify features surrounding San Bartolo, Guatemala (Saturno et al. 2007). However, these datasets were less useful in the neighbouring region of Ceibal, Guatemala (Garrison et al. 2008). Another limitation of the optical satellite images is that their acquisition is restricted to cloud-free conditions, which are rarely the case of the Yucatan peninsula (Geoghegan et al. 2004).

Figure 1. Ground picture of a former *sacbe*, showing a slightly raised road lined with white limestone.

The limitation of optical remote sensing can be overcome by using satellite radar images (e.g., Alos PalSAR, Sentinel-1, and Radarsat-2). Synthetic Aperture Radar (SAR) are active sensors that generate their own energy at generally longer microwave wavelengths and thus collect data independent of atmospheric conditions. Furthermore, microwave radiation is sensitive to differences in surface morphology, surface roughness, and soil moisture, all valuable properties for discriminating and mapping archaeological features (Lasaponara and Masini 2013). Also, their longer wavelengths (on the order of cm versus µm for the optical imagery) allow deeper penetration of the dense tropical forest canopy and thus offer the possibility of detecting sub-canopy features. Seasat L-HH band images were used to discover irrigation canals and cultivated wetlands in the Maya area (Adams 1980, Adams et al. 1981, Pope and Dahlin 1989, Pope and Dahlin 1993, Sever 1998). Elevation maps made with airborne radar imagery were also used to discover residential settlements around El Zotz in Guatemala with C-band imagery (Garrison et al. 2011) and monuments in Chunchucmil (Mexico) with L-band imagery (Hixson 2013).

Our study aims to map *sacbeob* that existed between Calakmul (Mexico), Uxul (Mexico), and El Mirador (Guatemala) with Landsat-5, 7, and 8 optical imagery and Sentinel-1, and Alos-PalSAR radar images. More specifically, it will 1) join the segments of *sacbeob* that were mapped by a field survey around El Mirador (Graham, 1967) or with Landsat-5 TM images around Calakmul (Folan et al. 1995) in the northern Peten region of the interior Maya Lowlands, extending from southern Campeche into Peten, Guatemala and 2) find new *sacbeob* nearby. As shown by the literature review, adding radar images in the analysis should improve the detection of man-made features such as *sacbeob* under dense tropical forests. The satellite images will be used in various RGB (Red, Green, and Blue) composites that will be photo-interpreted.

2. METHODOLOGY

2.1 Study area

The study area covers 2500 km^2 inside the Calakmul Biosphere Reserve closed to Campeche (Mexico), and the Maya Biosphere Reserve closed to Petén (Guatemala) (Figure 2). The natural vegetation is a dense tropical forest that has wetland areas called *bajos*. Three well-known ancient Maya cities exist in this area: Calakmul, El Mirador, and Uxul. The area also has several small Maya settlements (Witschey and Brown 2017). The area's topography is relatively flat in the western part and is rougher in the eastern part, with some hills having 350 m above sea level, as shown by the elevation map (Figure 2).

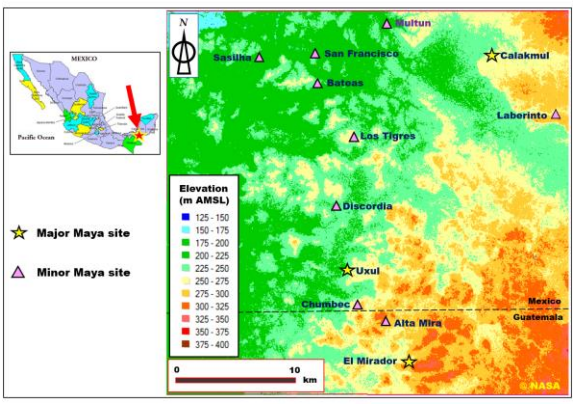

Figure 2. Location of the study area, associated elevation map, and location of some known ancient Maya sites

2.2 Imagery

This study used five types of imagery acquired during the dry season because Garrison et al. (2008) already showed that dry season images are better for detecting man-made structures in tropical forests. The first imagery was Landsat optical images. A Landsat-5 image was acquired with the Thematic Mapper (TM) sensor on January 24, 2015. A Landsat-7 image was taken with the Enhanced Thematic Mapper (ETM+) sensor on March 27, 2000. Both have six optical bands. Finally, a Landsat-8 image was acquired on March 31, 2016, with the Operational Land Imager (OLI) sensor that has seven optical bands. These images were selected because they have less than 1% cloud cover and were directly downloaded from the Global Visualization Viewer of the United States Geological Survey (http://glovis.usgs.gov/). The presence of infrared bands in this imagery is essential because they are particularly sensitive to the moisture content of the surface vegetation (Meingast et al. 2014). The Landsat imagery was processed to produce bottom-of-atmosphere reflectance images by removing the atmospheric effect with the ATCOR program in PCI Geomatica Banff (PCI Geomatics 2020), which uses the algorithm of Richter (2010). The original bands from these satellites have a spatial resolution of 30 m but, for the Landsat-7 ETM+ and the Landsat-8 OLI images, they were pan-sharpened with the panchromatic band to generate an image having a spatial resolution of 15 m, using the PANSHARP program of PCI Geomatica Banff (PCI Geomatics 2020) that applies the method of Zhang (2002a, 2002b).

The first SAR data is an Alos-1-PalSAR L-band radar image acquired on May 31, 2008, and downloaded from the Alaska Satellite Facility (https://www.asf.alaska.edu/). The imagery file contains two images: the HH (horizontal transmit and horizontal receive) and HV (horizontal transmit and vertical receive) polarized intensity images. This image was acquired with an incidence angle varying between 8 to 60°. It has a 12.5 m spatial resolution. The sensor has a long wavelength (23.62 cm) that should allow deep beam penetration under the vegetation cover (Nguyen et al. 2016). The second SAR image is a Sentinel-1A C-band radar image downloaded from the ESA Copernicus Open Access Hub (https://scihub.copernicus.eu/). This image was acquired on May 8, 2016. Each imagery file contains two images: the VV (vertical transmit and vertical receive) and the VH (vertical transmit and horizontal receive) polarized intensity images. The image was acquired with an incidence angle between 18.3 to 46.8°. It has a 10 m spatial resolution. The beam wavelength is 5.55 cm. Both radar images were acquired during an ascending east-looking orbit. They are helpful in this study because the backscatter is sensitive to variations in the soil moisture across a range of soil and vegetation conditions (Kasischke et al. 2009) and *sacbe* are usually drier than the surrounding area because they are made of limestone and are raised. All the downloaded images were displayed as an RGB composite and then visually photo-interpreted to delineate linear features interpreted either as clearcut, access roads, or *sacbe* segments by first delineating the *sacbeob* mapped by Graham (1967) and by Folan et al. (1995) (Figure 3). From the segments previously mapped, we tried to join them by looking for linear features which can appear by photo-interpreting the various image composites.

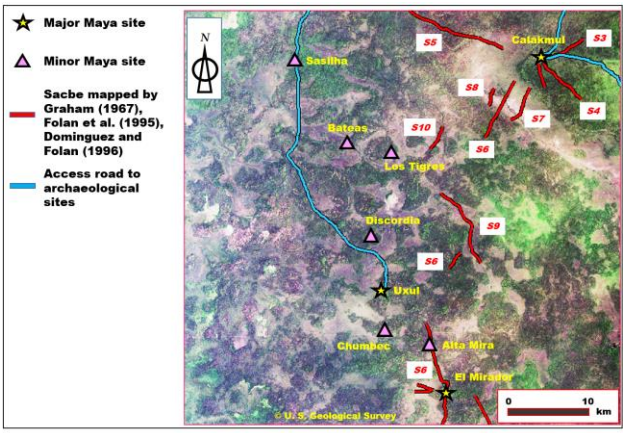

Figure 3. Previously mapped *sacbe* segments with some known ancient Maya sites.

3. RESULTS AND DISCUSSION

Sacbeob can be found in *bajos*, i.e., seasonally flooded depressions or forested areas. *Sacbe* segment #7 of Folan et al. (1995) found inside a *bajo* is very well visible on a true-colour RGB composite image made with the Landsat-5 TM image acquired in January 2015 (Figure 4a) and with the Landsat-8 OLI image acquired in March 2016 (Figure 4b). The location of the ancient *sacbe* can be determined by the tree alignment found inside the *bajo*, while the depression is covered by short-grass vegetation. This *sacbe* can also be delineated in the two false-colour RGB composites image made with the infrared bands, i.e., NIR (Near-Infrared) band (B5) and both SWIR (Shortwave-Infrared) bands (B6 and B7) of the Landsat-8 OLI image (Figures 5a and 5b). In both composite images, the difference in moisture between the vegetation growing over the *sacbe* and the one covering the bajo highlights the location of the raised causeway.

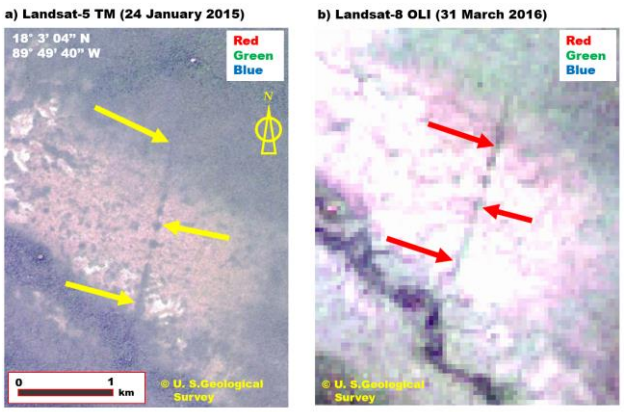

Figure 4. *Sacbe* segment #7 of Folan et al. (1995) located inside in a *bajo*, as displayed: a) on a Landsat-5 TM true-colour composite acquired in January 2015; b) on a Landsat-8 OLI true-colour composite made with the image acquired in March 2016.

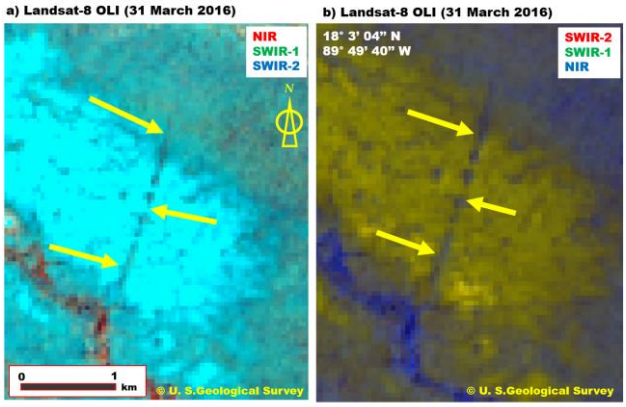

Figure 5. *Sacbe* segment #7 of Folan et al. (1995) located inside a *bajo*, as displayed: a) on the Landsat-8 OLI false-colour composite made with the image acquired in March 2016 (near-infrared band in red, first shortwave infrared band in green, and second shortwave infrared band in blue) and b) on a Landsat-8 OLI false-colour composite made with the same image (second shortwave infrared band in red, first shortwave infrared band in green, and near-infrared band in blue).

Figure 6 shows the same *sacbe* segment on two false-colour composites made with the radar image acquired at the end of the dry season. For Sentinel-1A, the C-VH polarized image is displayed in the red and blue channels, while the C-VV polarized image is displayed in the green channel (Figure 6).

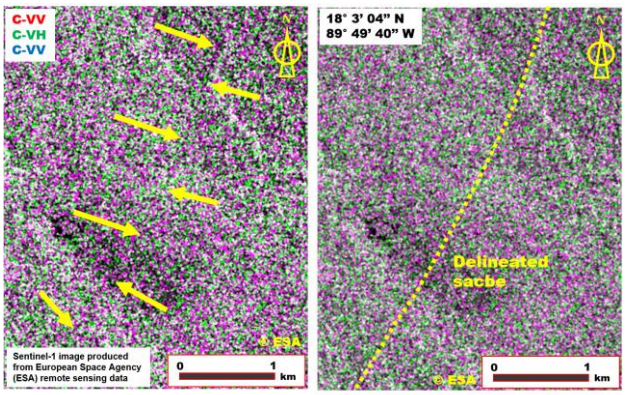

Figure 6. *Sacbe* segment #7 of Folan et al. (1995) found inside a *bajo* and surrounding forest area, as displayed on two false-colour composites made with the radar image acquired at the end of the dry season, with the Sentinel-1 image (C-VH band in red and blue, C-VV band in green).

For the Alos-1 PalSAR imagery, in Figure 7, the L-HV polarized image is displayed in the red and blue channels, while the L-HH polarized image is displayed in the green channel. By contrast to the optical composites, the *sacbe* section crossing the *bajo* is less visible on the radar composites because the radar beam is too penetrating for differentiating the vegetation cover of the *bajo* from the one over the *sacbe* as it directly reaches the ground. In the forested section, the segment of *sacbe* is more visible on the radar composites. This can be explained by the double-bounce scattering produced by the difference in the vegetation density and the difference between the treetop and the soil surface.

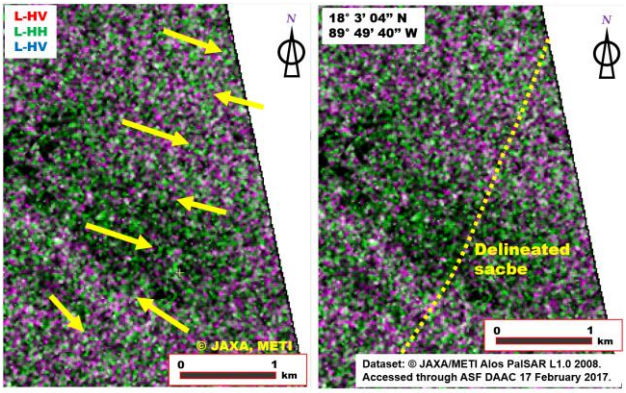

Figure 7. *Sacbe* segment #7 of Folan et al. (1995) found inside a *bajo* and surrounding forest area, as displayed on two false-colour composites made with the radar image acquired at the end of the dry season: a) Sentinel-1 (C-VH in red and blue, C-VV in green), and b) Alos-1 PalSAR (L-HV band in red and blue, L-HH band in green).

When located in a forested area, the *sacbe* is not visible on true-colour composite made with Landsat-7 ETM+ bands (Figure 8a) nor on the false-colour composite made with the Landsat-8 OLI bands (Figure 8b), as shown by the gap between two segments of *Sacbe* #6 (S6) of Folan et al. (1995). The dense forest canopy is an obstacle to detecting the hidden *sacbe*.

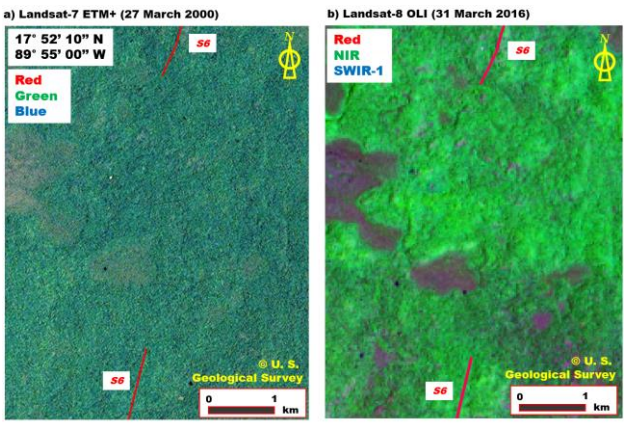

Figure 8. Gap between the two *Sacbe* #6 segments of Folan et al. (1995) located in a forested area, as displayed: a) on a Landsat-7 ETM+ true-colour composite (red band in red, green band in green, and blue band in blue) made with the image acquired in March 2000 and, b) a Landsat-8 OLI false-colour composite (red band in red, near-infrared band in green, and first shortwave infrared band in blue) made with the image acquired in March 2016.

Fortunately, the connection between these two segments is more visible on the false-colour composites made with either the Sentinel-1A (Figure 9) or the Alos-1 PalSAR image (Figure 10). On these two composite images, the assumed position of the sacbe is delineated by a straight line on the image. Such a line could be explained by the difference in the soil moisture between the drier causeway built with limestone and the surrounding crossed by the *sacbe*. This line is more visible on the Sentinel-1A image, probably because the VV polarization is more suitable than the HH polarization to detect *sacbeob* in densely forested areas. Also, the Sentinel-1A image was acquired with a C-band sensor with a shorter wavelength (5.55 cm) than the L-band (23.62 cm) of Alos-1 PalSAR. Hixson (2013) already noticed that longer wavelength radar beams are not as good as short-wavelength radar beams for detecting man-made structures in the Yucatan dense tropical forests because of the interference of the longer wavelength radar beams with the natural elements beneath the canopy.

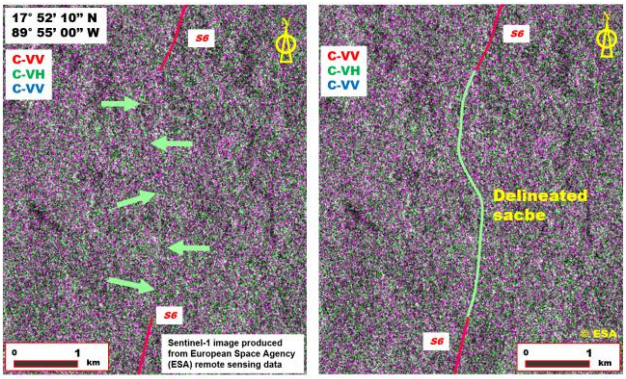

Figure 9. Connection between the two *Sacbe* #6 (S6) segments of Folan et al. (1995) located inside a forested area, as displayed on a false-colour composite made with the Sentinel-1A radar image (C-VH band in the red and blue, C-VV band in the green) acquired in May 2016. The location of the *sacbe* is indicated on the left panel by green arrows.

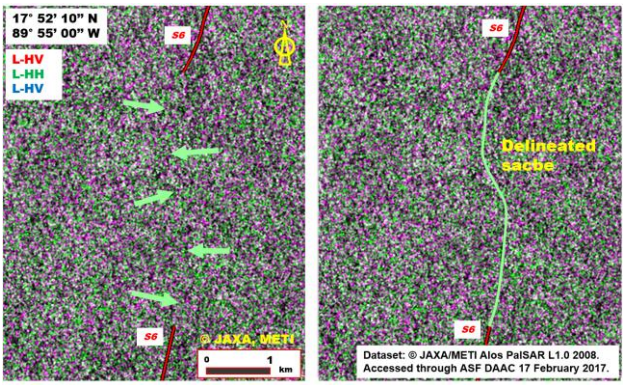

Figure 10. Connection between two segments of Sacbe #6 (S6) of Folan et al. (1995) located inside a densely forested area, as displayed on a false-colour composite made with the Alos-1 PalSAR radar image (L-HV band in the red and red, L-HH band in the green) acquired in May 2016: The location of the sacbe is indicated on the left panel by green arrows.

Besides *sacbeob*, there are also modern roads for accessing archaeological sites in the study area. One *sacbe* segment of Folan et al. (1995) coexists with an access road is *Sacbe* #3, just east of the site of Calakmul. The *sacbe* and the road are both located in a forested area. They appear differently on a WorldView-2 image acquired on January 25, 2015 (i.e., during the dry season) and displayed in Google Earth (Figure 11). The location of the *sacbe* is shown by trees having their top higher than the neighbouring forest. By contrast, the road is delineated by a wavy vegetation clearing in the dense canopy. This difference is not apparent on the Landsat images because of the lower spatial resolution of the image (15 m or 30 m) compared to the 0.4 m for the WorldView-2 image.

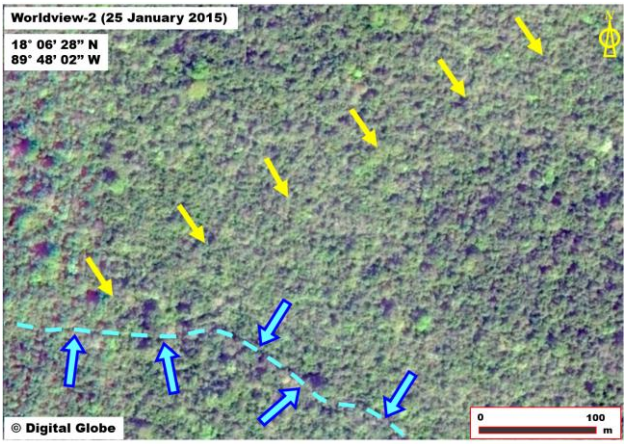

Figure 11. Comparison between an access road (blue arrows) and the nearby *sacbe* segment #3 (yellow arrows) of Folan et al. (1995), located in a forested area on a WorldView-2 true-colour composite acquired in January 2015 and displayed on Google Earth. The location of the sacbe is indicated by yellow arrows.

By contrast, the *sacbe* segment can be differentiated from the access road in the two false-colour composites made with Sentinel-1A images acquired during the dry season. The first one is made with the C-VH image in the red and blue channels, and the C-VV image in the green channel (Figure 12), and the second one with the opposite combination of polarization (Figure 13). Both images detect a straight line crossing the canopy at the same place where the trail was walked. The detection of this *sacbe* with the Sentinel-1A image can be explained by the difference in the vegetation height and the moisture difference between the *sacbe* and the surrounding.

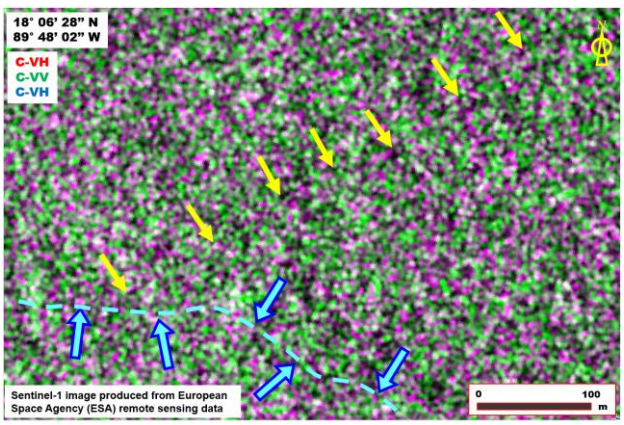

Figure 12. Comparison between an access road (blue arrows) and the nearby *sacbe* segment #3 (yellow arrows) of Folan et al. (1995) located in a forested area on a false-colour composite made with the Sentinel-1A image acquired in May 2016, with the C-VH image in red and blue, and the C-VV image in green. The location of the sacbe is indicated by yellow arrows.

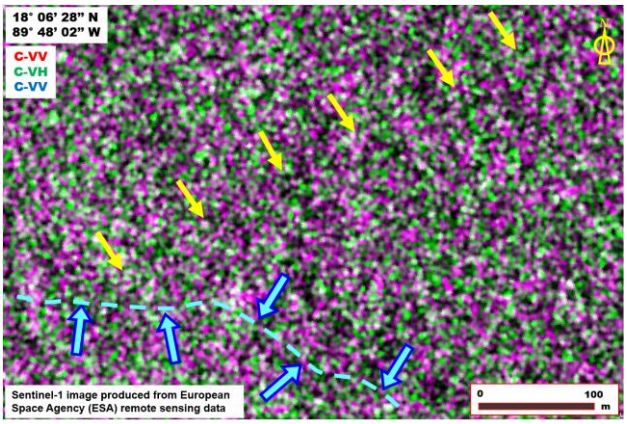

Figure 13. Comparison between an access road (blue arrows) and the nearby *sacbe* segment #3 (yellow arrows) of Folan et al. (1995) located in a forested area on a false-colour composite made with the Sentinel-1A image acquired in May 2016, with the C-VV band in red and blue, C-VH band in green. The location of the sacbe is indicated by yellow arrows.

The network of *sacbeob* delineated by photointerpretation of all the Landsat-5 TM, Landsat-7 ETM+, Landsat-8 OLI, Sentinel-1a, and Alos-1 PalSAR imagery is presented in figure 14. This network joins the *sacbe* segments of Graham (1967) and Folan et al. (1995) and allows to join the major ancient Maya sites of the area. Such delineation of *sacbeob* was also helpful to locate four potential ancient Maya sites, as detailed in LaRocque et al. (2019).

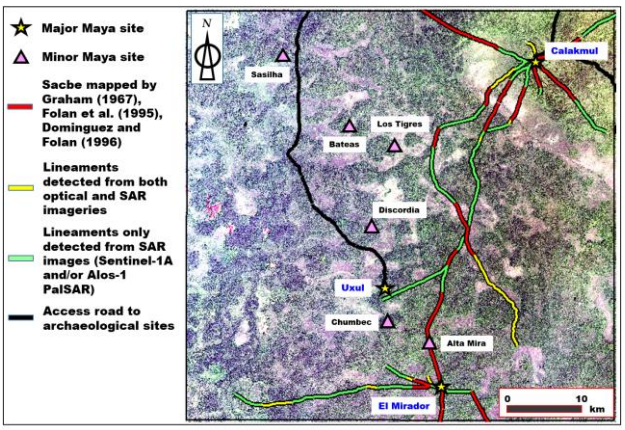

Figure 14. Network of lineaments corresponding probably to *sacbeob* mapped in the study area, from the photointerpretation of Landsat-5 TM, Landsat-7 ETM+, Landsat-8 OLI, Sentinel-1a, and Alos-1 PalSAR imageries, together with the *sacbe* segments of Graham (1967) and Folan et al. (1995), the access roads to the Uxul and Calakmul archaeological sites, as well as some Maya sites of the study area.

4. CONCLUSION

This study was able to map the connections between *sacbeob* segments, which were already delineated by Graham (1967) and Folan et al. (1995) between three major Maya cities, Calakmul and Uxul (Mexico), and El Mirador (Guatemala). We used optical satellite images that include Landsat-5, -7, and -8 images and Sentinel-1 C-VH and C-VV and Alos-1 PalSAR L-HH and L-HV radar images. The combination of their different bands produces composites that are helpful to distinguish many linear

features hidden by the dense canopy of the area and possibly related to ancient Maya *sacbe*. The physical properties of the *sacbeob* helped the mapping. Indeed, *sacbeob* are linear features, generally made of limestone and slightly higher in elevation than the surrounding topography and therefore drier. We were able to join the *sacbe* segments mapped by Graham (1967) and Folan et al. (1995). *Sacbeob* can be more easily detected on optical images in *bajos*, but SAR images are required to map them in forested areas because their longer wavelengths allow them to pass through the dense canopy and even reach the ground. In addition, the dryness of the *sacbeob* can be detected using SAR images, given that the intensity of the signal return is affected by the soil moisture. This study showed that the Sentinel-1 C-VV and C-VH imagery was more valuable than the Alos-1 PalSAR L-HH and L-HV imagery, likely because of the difference in the polarization and the wavelength of the radar beam. The C-band wavelength seems more appropriate than the L-band wavelength because longer radar beams can provide direct or double-bounce backscatters from natural structures beneath the canopy, acting as interferences.

Our method was developed on already documented *sacbeob*, but it needs to be tested on other potential *sacbeob* in another area with the same vegetation condition. Also, there is the need to validate the method with LiDAR data, such as in Chevance et al. (2019). The results of this study were obtained by photointerpretation of various image composites, and further work is needed to develop a more automated image analysis method, particularly those designed for lineament mapping. Hanus and Evans (2015) proposed a method for semi-automated pond extraction from LiDAR data in tropical forests. Monna et al. (2021) proposed a deep learning method to detect built cultural heritage from satellite imagery in tropical forests, but the canopy is not as dense as in our study area. Our study only uses the spectral or intensity information of the images, and additional work is needed to test whether textural variables will be helpful for such a mapping. In addition, numerous lineaments were also detected, but most of them could be related to more recent forest exploitation. Despite the low accessibility of the studied area, fieldwork should be useful to determine the former or the current usage of the detected lineaments.

ACKNOWLEDGMENTS

The authors would like to thank Adrien Jalran and Damien LaRocque for their help in image processing. The study was funded by UNB funds awarded to Prof. Leblon. The Landsat images were provided by the United States Geological Survey (USGS) and downloaded from the USGS Global Visualization Viewer website (https://glovis.usgs.gov/). The Sentinel-1A imagery was provided by the European Space Agency (ESA) and downloaded from the Copernicus Open Access Hub website (https://scihub.copernicus.eu/). The Alos-1 PalSAR image was provided by the Japan Aerospace Exploration Agency (JAXA) and downloaded from the Alaska Satellite Facilities (ASF) website (https://asf.alaska.edu/).

REFERENCES

Adams, R.E.W., 1980. Swamps, canals, and the locations of Ancient Maya cities. *Antiquity*, 54(212), 206–214.

Adams, R, Brown, E.W., Culbert, T., 1981. Radar mapping, archeology, and ancient Maya land use. *Science* 213, 1457–1463.

Bolles, D.D., Folan, W.J., 2001. An analysis of roads listed in colonial dictionaries and their relevance to pre-Hispanic linear features in the Yucatan peninsula, *Ancient Mesoamerica* 12, 299-314.

Canuto, M.A., Estrada-Belli, F., Garrison, T.G., Houston, S.D., Acũna, M.J., Kováč, M., Marken, D., Nondédéo, P., Thomas, L.A., Castanet, C., Chatelain, D., Chiriboga, C.R., Drápela, T., Lieskovský, T., Tokovinine, A., Velasquez, A, Fernández-Diaz, J.C., Shrestha, R., 2018. Ancient lowland Maya complexity as revealed by airborne laser scanning of northern Guatemala. *Science* 361 (6409), aau0137.

Chase, A.F., Chase, D.Z., Weishampel, J.F., Drake, J.B., Shrestha, R.L., Slatton, K.C., Awe, J.J., Carter, W.E., 2010. Airborne LiDAR, archaeology, and the ancient Maya landscape at Caracol, Belize. *J Archaeol Sci* 38(2), 387-398.

Chase, A.F., Chase, D.Z., Weishempel, F.F., 2013. The use of LiDAR at the Maya site of Caracol, Belize, 187-197. In Comer, D.C., Harrower, M.J. (Eds.). *Mapping archaeological landscapes from space*. Springer Briefs in Archaeology book series, New York, volume 5.

Chase, D.Z., Chase, A.F., Awe, J.J., Walker, J.H., Weishampel, J.F., 2011. Airborne LiDAR at Caracol, Belize (sic) and the interpretation of ancient Maya society and landscape. *Research Reports in Belizean Archaeology* 8, 61-73.

Chevance, J.-B., Evans, D., Hofer, N., Sakhoeun, S., Chhean, R., 2019. Mahendraparvata: an early Angkor-period capital defined through airborne laser scanning at Phnom Kulen. *Antiquity* 93(371), 1303-1321.

Comer, D.C., Harrower, M.J. (Eds.), 2013. *Mapping archaeological landscapes from space*. Springer Briefs in Archaeology book series, New York, volume 5.

Dominguez, M.R., Folan, W.J., 1996. Calakmul, México: Aguadas, bajos, precipitación y asentamiento en el Petén Campechano, 147-173. In Laporte, J.P., Escobedo, H. (Eds). *IX Simposio de Investigaciones Arqueológicas en Guatemala*, 1995. Museo Nacional de Arqueología y Etnología, Guatemala.

Folan, W.J., Marcus, J., Miller, W.F., 1995. Verification of a Maya settlement model through remote sensing. *Camb Archaeol J* 5, 277-283

Garrison, T.G., Houston, G., Golden, S.D., Inomata, T., Nelson, Z., Munson, J., 2008. Evaluating the use of IKONOS satellite imagery in lowland Maya settlement archaeology. *J. Archaeol Sci* 35(10), 2770–2777.

Garrison, T.G., Chapman, B., Houston, S., Roman, E., Garrido-Lopez, J.L., 2011. Discovering ancient Maya settlements using airborne radar elevation data, *J. Archaeol Sci*, 38(7), 1655-1662.

Geoghegan, J., Schneider, L., Vance, C., 2004. Spatially explicit, statistical land-change models in data-sparse conditions, 247-270. In Turner, B.L. II, Geoghegan, J., Foster, D.R. (Eds.). *Integrated land-change science and tropical deforestation in the southern Yucatán*. The Clarendon Lectures in Geography and Environmental Studies.

Graham, I, 1967. Archaeological explorations in El Peten, Guatemala. Tulane University, New Orleans, Middle American Research Institute 33.

Hanus, K., Evans, D., 2016. Imaging the waters of Angkor: A method for semi-automated pond extraction from LiDAR data. *Archaeol Prospect* 23(2), 87-94.

Hixson, D.R., 2013. The use of multispectral imagery and airborne synthetic aperture radar for the detection of archaeological sites and features in the western Maya wetlands of Chunchucmil, Yucatan, Mexico, 133-144. In Cormer, D.C., Harrower, M.J. (Eds). *Mapping Archaeological Landscapes from Space*, Springer Briefs in Archaeology Book series, volume 5.

Inomata, T., Pinzón, F., Ranchos, J.L, Haraguchi, T. Nasu, H., Fernández-Diaz, J.C., Aoyama, K., Yonenobu, Y., 2017. Archaeological application of airborne LiDAR with Object-Based vegetation classification and visualization techniques at the Lowland Maya site of Ceibal, Guatemala. *Remote Sensing* 99(561); doi:10.3390/rs9060563.

LaRocque, A., Leblon, B., Ek. J., 2019. Detection of potential large Maya settlements in the northern Petén area (State of Campeche, Mexico) using optical and radar remote sensing. *J Archaeol Sci: Reports* 23 (2019), 80–97.

Lasaponara, R., Masini, N., 2013. Satellite synthetic aperture radar in archaeology and cultural landscape, an overview. *Archeol. Prospect.* 20(2), 71–78.

Magnoni, A., Stanton, T.W., Barth, N., Fernández-Diaz, J.C., León, J.F.O., Ruíz, F.P., Wheeler, J.A., 2016. Archaeological features in airborne Lidar Data from central Yucatán. *Advances in Archaeological Practice* 4(3), 232–248.

Meingast, K.M., Falkowski, M.J., Kane, E.S., Potvin, L.R., Benscoter, B.W., Smith, A.M.S., Bourgeau-Chavez, L.L., Miller, M.E., 2014. Spectral detection of near-surface moisture content and water-table position in northern peatland ecosystems. *Remote Sens Environ* 152, 536-546.

Monna, F., Rolland, T., Denaire, A., Navarro, N., Granjon, L., Barbé, R., Chateau-Smith, C., 2021. Deep learning to detect built cultural heritage from satellite imagery. Spatial distribution and size of vernacular houses in Sumba, Indonesia. *J Cult Herit* 52, 171-183.

Nguyen, L.V., Tateishi, R., Nguyen, H.T., Sharma, R.C., To, T.T., Le, S.M., 2016. Estimation of Tropical Forest Structural Characteristics Using ALOS-2 SAR Data. *Adv Rem Sens* 2016 (5), 131-144.

PCI Geomatics, 2020. PCI Geomatica® Software, Version Banff Edition, Markham, ON, Canada.

Pope, K.O, Dahlin, B.H., 1989. Ancient Maya wetland agriculture: New insights from ecological and remote sensing research. *J. Field Archaeol* 16(1), 87–106.

Pope, K.O, Dahlin, B.H., 1993. SAR detection and ecology of Ancient Maya canal systems – reply to Adams et al. *J. Field Archaeol* 20, 379–383.

Prufer, K.M., Thompson, A.E., Kennett, D.J., 2015. Evaluating airborne LiDAR for detecting settlements and modified landscapes in disturbed tropical environments at Uxbenká, Belize. *J Archaeol Sci* 57, 1-13

Richter, R., 2010. Topographic Correction for Satellite Imagery - ATCOR2/3 User Guide). DLR - German Aerospace Center.

Saturno, W., Sever, T.L., Irwin, D., Howell, B., Garrison, T.G, 2007. Putting us on the map: remote sensing investigation of the ancient Maya landscape, 137–160. In Wiseman, J., El-Baz, F. (Eds.). *Remote sensing in archaeology: interdisciplinary contributions to archaeology*. Springer Science and Business Media.

Sever, T.L., 1998. Validating prehistoric and current phenomena upon the landscape of the Petén, Guatemala, 145–163. In Liverman, D., Moran, E.F., Rindfuss, R.R., Stern, P.C. (Eds.). *People and pixels: Linking remote sensing and social science*. National Academy Press.

Shaw, J., 2001. Maya *sacbeob*: form and function. *Ancient Mesoam* 12, 261-272.

Shaw, J.M., 2008. White roads of the Yucatán: changing social landscapes of the Yucatec Maya. The University of Arizona Press, Tucson (USA).

Solberg, S., Weydahl, D.J., Næsset, E., 2007. SAR forest canopy penetration depth as an indicator for forest health monitoring based on leaf area index LAI. In: Proc. 5th Int. Symp. Retrieval of Bio- and Geophysical Parameters from SAR Data for Land Applications, (5 pp.). (Bari Italy).

Thompson, A.E., 2020. Detecting Classic Maya settlements with Lidar-derived relief visualizations. *Remote Sensing* 12(2838), doi:10.3390/rs12172838.

Wiseman, J., El-Baz, F. (Eds.), 2007. Remote sensing in archaeology. Springer, New York.

Witschey, W.R.T., Brown, C.T., 2017. The Electronic Atlas of Ancient Maya Sites. http://MayaGIS.smv.org [Electronic database graciously sent by the first author, January 19, 2017].

Zhang, Y., 2002a. A new automatic approach for effectively fusing Landsat 7 as well as IKONOS images. *Int Geosci Remote Se*, 2002, 2429-2431.

Zhang, Y., 2002b. Problems in the fusion of commercial high-resolution satellite as well as Landsat 7 images and initial solutions. *Int. Arch Photogramm. Remote Sens. Spat. Inf. Sci.* 34, 587–592.